

<https://doi.org/10.33271/nvngu/2026-1/120>

Thuy Thi Hoang,  
orcid.org/0009-0005-5181-9379,  
Anh Tuan Luu\*,  
orcid.org/0009-0001-7738-9718

Hanoi University of Mining and Geology, Faculty of Geomatics and Land Administration, Hanoi, Socialist Republic of Vietnam

\* Corresponding author e-mail: [luuanhtuan@humg.edu.vn](mailto:luuanhtuan@humg.edu.vn)

## LARGE-SCALE TOPOGRAPHIC MAPPING OF VEGETATION AREAS BASED ON UAV AND GNSS TECHNOLOGY

**Purpose.** To develop a method for generating accurate large-scale topographic maps in densely vegetated areas using UAV (Unmanned Aerial Vehicle) and GNSS (Global Navigation Satellite System) technologies. The focus is on correcting elevation data from UAV imagery through a polynomial model based on CORS checkpoints.

**Methodology.** The research was conducted in Mai Pha commune, Lang Son province, Vietnam. A DJI Phantom 3 Pro UAV was used to capture aerial images, and GNSS-RTK (CORS) technology was employed to collect ground control points. A polynomial surface fitting method (1st to 3rd degree) was applied to model vegetation thickness and correct the digital surface model (DSM) to obtain a digital elevation model (DEM). The DSM was smoothed using various radii (0; 20; 50; 70; 100 m), and the accuracy was assessed using different numbers of checkpoints (150; 350; 1,000). A software module was developed to automate the correction process.

**Findings.** The accuracy of the DEM improved with an increased number of checkpoints and an appropriate smoothing radius. The best results were achieved with 1,000 checkpoints and a smoothing radius of 50 m. The corrected DEM achieved elevation accuracy within 1–2 meters, meeting regulatory standards for large-scale topographic maps (1:2,000–1:5,000). The method proved effective even in areas with dense vegetation, where traditional mapping methods face limitations.

**Originality.** This study introduces a novel approach that integrates UAV photogrammetry with GNSS-RTK data and polynomial surface modeling to correct elevation data in vegetated areas. The developed software module automates the correction process, enhancing efficiency and consistency.

**Practical value.** The proposed method enables the creation of accurate, large-scale digital topographic maps in challenging environments with dense vegetation. It offers a cost-effective and efficient alternative to traditional surveying methods, with potential applications in forestry, land management, and infrastructure planning.

**Keywords:** *UAV, GNSS technology, vegetation areas, large-scale topographic map*

**Introduction.** Terrain maps provide helpful information about the topography through contour lines and DTM, as well as precise and comprehensive visuals that depict both natural and artificial elements on the ground [1]. Topographic maps are utilized in various fields, including agriculture [2] and disaster management [3]. Several pieces of equipment have been employed in land surveying to create terrain mapping, such as traditional methods (clinometers, levels, and theodolites) [4], light detection and ranging radar (LiDAR) [5], terrestrial laser scanning (TLS) [6], human-crewed aircraft [7], and remote sensing [8]. Despite their many advantages, these methods have various drawbacks, particularly in terms of usage, time consumption, and cost [9]. In recent years, the use of drones to collect remote sensing data for the production of large-scale topographic maps has become increasingly popular due to their affordability and usefulness. UAVs offer several advantages, including rapid data collection, low cost, high precision, and the ability to collect data in challenging environmental conditions [10].

Various UAV types have been demonstrated to be accurate in conducting topographic surveys worldwide [11, 12]. According to [1], UAV photogrammetry may be used to create terrain maps, digital terrain models, digital surface models, digital maps, and orthophotos that all meet international standards. The study indicated that, because the accuracy achieved was within acceptable bounds, UAV photogrammetry for large-scale topographic mapping may successfully replace existing techniques, such as GPS and total stations. In addition to assessing the accuracy, several studies have also been conducted to confirm the time and cost-effectiveness of this technology in creating topographic maps. [13] described briefly the procedure for establishing a large-scale terrain map of the Universiti Teknologi Malaysia campus, Malaysia. The findings showed that, depending on the location, photogrammetry software could produce an accurate, large-scale topographic map in less than a week. With the above advantages, many studies have applied this technology to survey terrain. Many publications have used UAV images to create large-scale topographic maps with great detail of small regions with

uncomplicated and accessible terrain [13–15]. Others have found UAVs to be a valuable technology for mapping hard-to-reach areas, such as mining sites [16], flooded areas [17], river topography [18], and deep gorges [19, 20]. However, these studies have primarily focused on areas with limited vegetation cover. For areas with thick vegetation cover, mapping remains challenging because there are not many visible ground surfaces. To address the challenges of topographic mapping under dense vegetation, [21] developed a cost-effective photogrammetric UAV system. The study's findings demonstrate that mapping topography beneath a dense canopy of vegetation is possible by combining GPS field surveys and UAV data. In another study, [22] used a UAV-LiDAR system with an appropriate filtering technique to acquire high-resolution topographic data in vegetated areas.

Although the obtained results indicated that the survey using a UAV system helps gather high-resolution topographic data at heavily wooded locations, the amount of research on this issue is limited. Additionally, existing studies have not yet provided specific technical solutions for the process and technical standards required to create large-scale maps using UAV technology.

In this research, the author proposes a solution to calibrate the digital surface model (vegetation cover) derived from uncrewed aerial vehicle (UAV) image data, based on the test points measured by RTK dynamic GPS technology (CORS). From there, a topographic map of the research area is established. The research result is a software that automatically calibrates the elevation of the photo measurement points on the DSM (surface including vegetation cover) to the elevation of the terrain points. Experimental data have demonstrated the accuracy of the algorithm.

**Study area.** The study was carried out in the low-mountain and hilly landscape of Mai Pha commune, Dong Kinh ward, Lang Son city, Lang Son province, at coordinates 21°50'08"N, 106°46'19"E. Administratively, the study site is framed by Hoang Van Thu and Tam Thanh wards to the north, Mai Pha commune to the south, Vinh Trai ward to the east, and Chi Lang ward to the west. The mapped area is characterized by complex topography, primarily composed of low mountains and undulating hills, which together account for more than 80 % of the total surface. The mean elevation is approx-

imately 252 m above sea level. Still, local relief is pronounced: short slopes, benches and concave valley segments produce frequent elevation changes over short horizontal distances, creating a highly heterogeneous terrain mosaic (Fig. 1).

Climatically, the site is situated within the humid subtropical belt typical of northern Vietnam. Seasonal contrasts are distinct: a warm, wet monsoon season is followed by a cooler, drier winter. Due to the complex orography, these seasonal signals are spatially non-uniform; cold-air intrusions and orographic lifting produce rapid changes in temperature and humidity across short distances, resulting in substantial microclimatic variability. Such meteorological variability directly influences vegetation phenology and moisture status across the low-mountain landscape, contributing to a mixture of evergreen forest patches and areas that undergo seasonal changes.

Land cover in the research area is diverse. Natural and secondary forest stands, locally dominated by pine and eucalyptus, are interspersed with managed tree plantations and areas under tea cultivation. Agricultural plots, access tracks, and small settlement clusters are predominantly located along gentler slopes and valley bottoms, where soils are deeper and agricultural activities are concentrated. The heterogeneous composition of canopy types and ground surfaces yields strong spatial contrasts in surface reflectance and texture, both spectrally and structurally.

From the perspective of UAV-based data acquisition and topographic mapping, the study area presents several logistical and technical challenges. The mosaic of canopy architectures, tall, dense pine and eucalyptus stands adjacent to low-profile tea plantations, complicates image matching and ground point visibility for photogrammetric workflows. Dense canopies and shadowed slope aspects reduce the number of identifiable ground control features in vertical imagery, increasing the need for carefully distributed ground control points across elevation bands and along ridge and valley axes. Rapidly changing wind and weather conditions, particularly during transitional seasons, also constrain safe flight windows and can introduce motion blur or inconsistent illumination in the captured imagery.

Moreover, the steep and variable slopes increase the risk of occlusions, requiring lower flight altitudes or

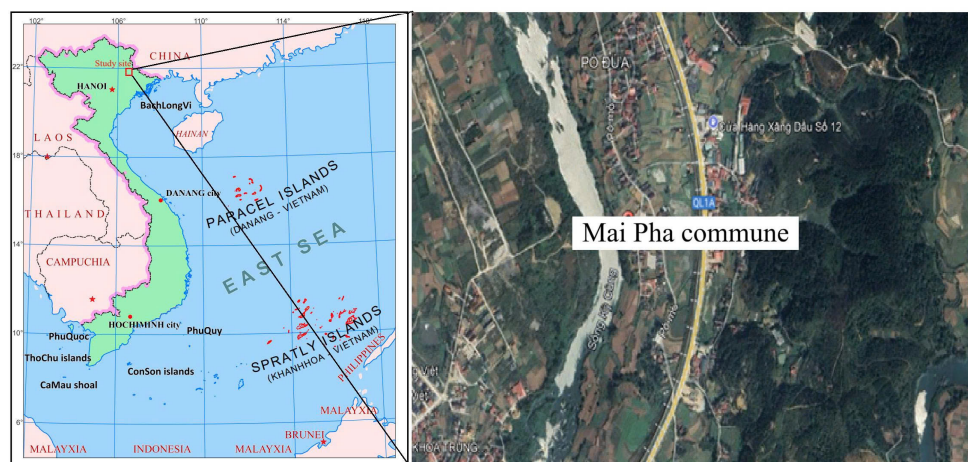


Fig. 1. The study area

higher image overlap to ensure sufficient stereoscopic coverage for digital surface model and digital terrain model generation. Vegetation heterogeneity further necessitates the use of multispectral sensors (or LiDAR, where available) to discriminate canopy types and to retrieve vegetation indices for health assessment. Taken together, the physiographic, climatic, and land-use characteristics of the Mai Pha study area necessitate a careful, adaptive UAV survey design, including tailored flight plans, robust ground control point placement, and appropriate sensor selection, to produce reliable topographic products and support downstream analyses of vegetation condition and agricultural management.

**Methodology and data collection. Data collection.** The study used a DJI Phantom 3 Pro drone, a device suitable for creating large-scale topographic maps, to capture images of the study area (Fig. 2). The Phantom 3 Pro is equipped with a 4K camera featuring a 1/2.3-inch sensor, enabling high-resolution photos and videos. The Phantom 3 Pro utilizes a GPS positioning system to help determine precise location and maintain stability when flying at high altitudes. This helps the aircraft fly along a predetermined path and collect geographic data efficiently. The 3-axis stabilization system helps the aircraft maintain a stable position during flight. Additionally, it supports automatic flight along set routes, saving time and energy. In particular, this type of aircraft connects to the phone via the DJI GO application, enabling users to view live images from the camera and remotely control the aircraft. The device has a flight time of up to 23 minutes and a flight distance of up to 5 km. Therefore, the aircraft can complete multiple missions continuously without needing a significant amount of time to stop for battery charging.

Aerial imaging software is used to create the flight route, ensuring the mapping meets accuracy standards. In this study, a *DJI Phantom 3 Pro* was used to capture 68 orthogonal JPEG photos at a height of 100 meters, with 80 and 75 % overlap in the front and side, respectively. The estimated time to complete the flight plan is 5 minutes 28 seconds. Fig. 3 illustrates the route planning and parameter settings for the study area.

After the planning of routes, the flight plan was transmitted to the UAV photography system in real-time. Aerial photography was conducted after the UAV system had been checked. The aircraft's condition was monitored using the ground station monitoring program, and the UAV would autonomously land when the flight was complete. The data were examined on the spot



Fig. 2. Experimental UAV aircraft in Lang Son

once the aerial photography flight was completed to determine whether any photos were missing and whether the number of photos and flight route characteristics were consistent. It is also important to check the photo quality to make sure there are no ambiguities. Fig. 4 shows a representative aerial image captured over the Lang Son experimental area, illustrating canopy heterogeneity, slope aspects, and surface textures that influence photogrammetric point matching and DSM quality. The imagery evidences mixed vegetation covers and interspersed clearings, highlighting why ground visibility is limited and why elevation correction must rely on GNSS-based checkpoints

Static techniques are used to measure the ground control point, or GCP, which is evenly distributed throughout the study area. Fig. 5 visually situates these GCPs within the study area, showing an even spatial spread along slope–valley transects and across elevation bands to stabilize least-squares estimation for second- and third-degree polynomial models.

Table 1 lists the Ground Control Points, including easting, northing, and elevation, which demonstrates a deliberately stratified network spanning approximately 278–310 m in elevation to anchor photogrammetric adjustments across heterogeneous low-mountain terrain.

The point IDs KCA1-KCA16 indicate a compact yet well-distributed control scheme designed to constrain polynomial surface fitting and reduce local biases from canopy occlusion when converting DSM to DEM. Table 1 (numerical coordinates) and Fig. 4 (spatial layout)



Fig. 3. Route planning and parameter setting



Fig. 4. Aerial photo taken at the Lang Son experimental area



Fig. 5. Dynamic GPS image control point diagram (CORS)

Table 1

Co-ordinates of Ground control points

Point number	Easting, m	Northing, m	Elevation, m
KCA1	451,092.699	2,417,004.242	288.957
KCA 2	451,094.128	2,416,953.17	286.026
KCA 3	451,121.595	2,416,843.908	277.975
KCA 4	451,114.730	2,417,096.278	292.871
KCA 5	451,138.632	2,417,027.615	299.778
KCA 6	451,171.580	2,417,033.605	302.057
KCA 7	451,261.933	2,417,061.426	310.402
KCA 8	451,167.399	2,416,933.138	305.049
KCA 9	451,198.234	2,416,932.536	304.423
KCA 10	451,241.507	2,416,922.217	303.387
KCA 11	451,279.959	2,416,934.439	303.823
KCA 12	451,146.387	2,416,965.258	303.578
KCA 13	451,137.821	2,416,935.911	301.541
KCA 14	451,106.929	2,417,122.343	291.501
KCA 15	451,136.186	2,417,162.646	291.606
KCA 16	451,150.093	2,417,192.136	289.839

demonstrate that the control network satisfies two key conditions for reliable elevation correction: dense coverage of relief variability and balanced geometry to mitigate error propagation during DSM smoothing and DEM derivation. This pairing also explains later accuracy gains at larger checkpoint counts and optimal smoothing radii, since robust, well-placed GCPs improve both georeferencing fidelity and the local regressions used to estimate vegetation thickness.

**Methodology.** In this study, the polynomial function problem was applied to determine the thickness of the vegetation cover. The thickness of the vegetation cover is the difference between the DSM obtained from the UAV flight results and the digital terrain model (DEM). The elevation of the terrain point is determined using CORS technology or a total station.

To calibrate the elevation of points determined by UAV technology, at each point, it is necessary to iden-

tify the function representing the vegetation cover for the terrain surface, as follows

$$Z_i = F(x_i, y_i), \quad (1)$$

where  $Z_i$  is the thickness of vegetation cover at coordinate position  $(x_i, y_i)$ .

Depending on the terrain, the function FFF is represented as a polynomial of degree 1, 2, or 3.

Polynomial function of degree 1 is

$$Z = Z_0 + Ax + By. \quad (2)$$

Polynomial function of degree 2 is

$$Z = Z_0 + Ax + By + Cx^2 + Dy^2 + Exy.$$

Polynomial function of degree 3 is

$$Z = Z_0 + Ax + By + Cx^2 + Dy^2 + Exy + Fx^3 + Hx^2y + Kxy^2.$$

To determine the coefficients of the polynomial function for each pixel, checkpoints are required. The number of checkpoints ranges from 3 to 10, depending on the degree of the polynomial. The higher the degree of the function, the greater the number of checkpoints needed, and vice versa. If the number of checkpoints exceeds the number of coefficients, the least squares method is applied to obtain the optimal coefficients.

The corrected numerical equation of the coefficients corresponding to the degrees of the function (2) can be expressed as:

- for the first-degree function

$$V_z = 1 \cdot \Delta Z_0 + x \cdot \Delta A + y \cdot \Delta B + l_z, \quad l_z = -Z; \quad (3)$$

- for the second-degree function

$$V_z = 1 \cdot \Delta Z_0 + x \cdot \Delta A + y \cdot \Delta B + x^2 \cdot \Delta C + y^2 \cdot \Delta D + xy \cdot \Delta E + l_z, \quad l_z = -Z;$$

- for the third-degree function

$$V_z = 1 \cdot \Delta Z_0 + x \cdot \Delta A + y \cdot \Delta B + x^2 \cdot \Delta C + y^2 \cdot \Delta D + xy \cdot \Delta E + x^3 \cdot \Delta F + l_z, \quad l_z = -Z.$$

In formula (3) the coefficients  $(A, B, C, D, E, Z)$  are represented as their approximate values plus correction terms

$$A = A_0 + \Delta A; \quad B = B_0 + \Delta B; \quad \dots; \quad Z = Z_0 + \Delta Z.$$

Applying the method of indirect adjustment, the coefficients of the model (3) can be determined. From these coefficients, the vegetation surface elevation can be corrected relative to the terrain surface elevation (4).

1. Error equation

$$V = AX + L. \quad (4)$$

2. Normal equation

$$A^TAX + A^TL = 0 \quad \text{or} \quad NX + B = 0.$$

3. Unknown vector

$$X = -N^{-1}B.$$

Finally, the corrected height of the vegetation cover relative to the terrain surface is expressed as

$$H_{dh} = H_{DSM} - Z. \quad (5)$$

The calibration process is carried out in two steps.

*Step 1: Smoothing the DSM surface model.* Since the vegetation surface generated from UAV imaging tech-

nology is very complex, there is no suitable numerical model, especially in large scale. To approximate the vegetation surface, the vegetation surface is smoothed by dividing the surface into square grids to determine the characteristic height for each location or determined at each pixel, through a polynomial function for each small area according to the radius selected to suit the specific terrain. The smoothing information needs to be selected during the implementation process.

By constructing a polynomial function according to formulas (1 and 2), the height of the vegetation cover at each pixel can be determined. The polynomial function is selected to be of degree 2 or degree 3. Based on the height of neighboring pixels, an approximate function is constructed, and then the height determined by the polynomial function corresponds to the pixel. The result of the height of the vegetation cover after smoothing will be close to a mathematical model for each aerial photography area.

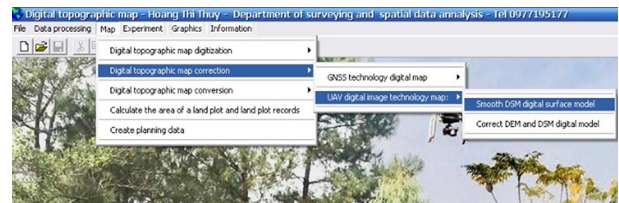
*Step 2: Determining the digital terrain model from the DSM (Digital Surface Model).* After the surface model of the vegetation cover has been smoothed, based on the elevation of each vegetation cover point and the terrain elevation of the nearest check points, the program module automatically builds a model to determine the vegetation cover thickness and terrain elevation for each corresponding pixel.

To perform this task, a program module for automatic calculation has been built to ensure accuracy and economic efficiency. The program interface is shown in Figs. 6, a, b. These figures present the custom software modules that operationalize the two-stage pipeline: a DSM smoothing interface and a DSM-to-DEM correction interface, respectively. These interfaces allow users to select the smoothing radius, polynomial degree, and checkpoint settings in a controlled workflow. The information determining the elevation of the terrain point to be selected is presented in Fig. 6, c. This Figure shows the parameter panel for terrain elevation selection, where the nearest CORS-based checkpoints are referenced to estimate vegetation thickness and correct pixel-wise heights, bridging UAV-derived DSM values to ground-truth DEM elevations.

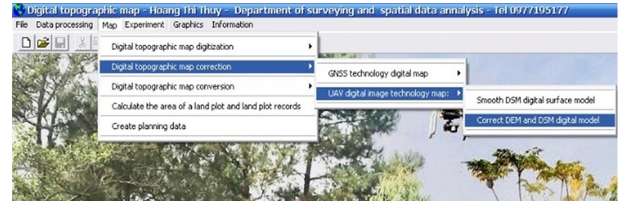
The program block diagram is shown in Fig. 7.

The main workflow illustrated in Fig. 7 can be summarized as follows. First, during data ingestion, the UAV-derived digital surface model (DSM) and CORS-based ground checkpoints are loaded, followed by initial quality control and coordinate consistency checks. Next, in the DSM smoothing step, a user-defined neighborhood radius is applied to suppress high-frequency canopy noise. Then, local polynomial fitting is performed: for each location, nearby checkpoints are selected, and a second or third-degree polynomial is fitted to estimate the local vegetation thickness. In the elevation correction stage, the estimated canopy thickness is subtracted from the smoothed DSM to obtain the digital elevation model (DEM) representing ground level. Finally, the validation and export step involves evaluating the DEM accuracy against independent measurements, fine-tuning model parameters if necessary, and exporting the final DEM along with diagnostic information.

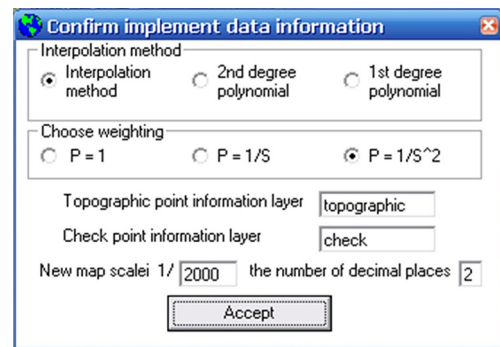
**Results and discussion. Reference DEM and DSM characteristics.** Fig. 8 presents the reference Digital El-



a



b



c

Fig. 6. Program interface and digital model modules:

a – digital surface model smoothing module; b – module for determining the digital terrain model from the DSM; c – information on selecting the digital terrain model

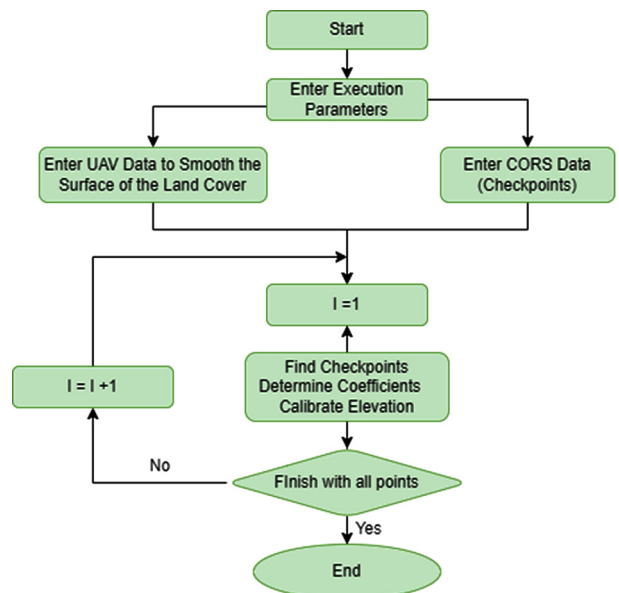


Fig. 7. Block diagram of the program execution

elevation Model, derived from direct total-station measurements, which serves as the ground truth against which UAV-based corrections are evaluated. The reference DEM displays pronounced micro-relief, including steep slope breaks, benches, and small valley segments, which typify the low-mountain/hilly morphology of the

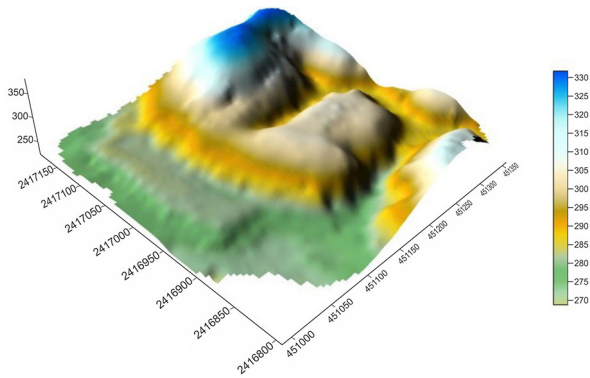


Fig. 8. Digital terrain model from direct measurement data in Lang Son City

study area and highlight the challenge of deriving bare-earth elevations beneath dense canopies.

The raw UAV-derived DSM shown in Fig. 8 exhibits the typical canopy-induced positive bias, where vegetation and tree canopies raise surface elevations well above the underlying terrain. The raw DSM contains high-frequency roughness associated with individual crowns and branches; this noise must be suppressed before reliable local regressions can estimate canopy thickness and recover the terrain surface. The sample point list in Table 2 illustrates this effect numerically: many DSM points have elevations that change after smoothing, indicating that local high-frequency cano-

py artifacts are effectively attenuated by the smoothing stage (Table 2).

The digital surface model of the vegetation cover, obtained using UAV technology, is shown in Fig. 9.

This Figure presents the raw UAV-derived DSM of vegetation cover, illustrating canopy-driven elevation biases. The coordinate data of some points on the vegetation cover can be derived through digital image processing software. Table 2 lists the sample coordinates and heights before and after smoothing, illustrating how a 50 m radius stabilizes local height estimates before polynomial fitting.

**Effect of smoothing radius: from DSM to smoothed DSM.** Smoothing the DSM is an essential preprocessing step that reduces canopy noise while retaining the larger-scale terrain signal. Fig. 10 shows the DSM after applying a 50 m smoothing radius: high-frequency fluctuations are visibly reduced while the broader topographic structure remains preserved.

Numerically, Table 2 documents the per-point changes before and after smoothing. Although point-by-point differences vary (dependent on local canopy density and slope), the overall effect is a convergence toward more stable local height estimates (Table 2). The comparison of multiple radii (0; 20; 50; 70; 100 m) enables assessment of the classical bias variance trade-off: minimal radii ( $R = 0-20$  m) preserve fine detail but retain canopy noise; large radii ( $R \geq 100$  m) over-smooth and may degrade terrain fidelity by removing legitimate micro-relief. The vi-

Table 2

Coordinates of vegetation cover points measured by UAV technology and coordinates of those points after smoothing

No.	Coordinates of vegetation cover points derived from UAV data			Coordinates of vegetation cover points after smoothing		
	X, m	Y, m	H, m	X, m	Y, m	H, m
1	2,416,951.805	451,202.769	306.000	2,416,951.805	451,202.769	309.28443
2	2,416,779.805	451,124.769	281.805	2,416,779.805	451,124.769	280.77804
3	2,416,779.805	451,122.769	283.066	2,416,779.805	451,122.769	280.87568
4	2,416,779.805	451,120.769	283.375	2,416,779.805	451,120.769	280.97434
5	2,416,779.805	451,118.769	283.106	2,416,779.805	451,118.769	281.08060
6	2,416,779.805	451,116.769	282.838	2,416,779.805	451,116.769	281.18097
7	2,416,779.805	451,114.769	282.596	2,416,779.805	451,114.769	281.28485
8	2,416,779.805	451,112.769	282.559	2,416,779.805	451,112.769	281.38334
9	2,416,779.805	451,110.769	282.575	2,416,779.805	451,110.769	281.45692
10	2,416,779.805	451,108.769	282.009	2,416,779.805	451,108.769	281.48957
...	...	...	...	...	...	...
42,470	2,417,257.805	451,142.769	276.820	2,417,257.805	451,142.769	277.11236
42,471	2,417,257.805	451,140.769	276.747	2,417,257.805	451,140.769	277.17691
42,472	2,417,257.805	451,138.769	276.674	2,417,257.805	451,138.769	277.19478
42,473	2,417,257.805	451,136.769	276.600	2,417,257.805	451,136.769	277.17672
42,474	2,417,257.805	451,134.769	276.527	2,417,257.805	451,134.769	277.14619
42,475	2,417,257.805	451,132.769	276.456	2,417,257.805	451,132.769	277.12105
42,476	2,417,257.805	451,130.769	276.388	2,417,257.805	451,130.769	277.09732
42,477	2,417,257.805	451,128.769	276.367	2,417,257.805	451,128.769	277.09387
42,478	2,417,257.805	451,126.769	276.058	2,417,257.805	451,126.769	277.10984
42,479	2,417,257.805	451,124.769	276.813	2,417,257.805	451,124.769	277.13587
42,480	2,417,257.805	451,122.769	276.763	2,417,257.805	451,122.769	277.16546
42,481	2,417,257.805	451,120.769	276.530	2,417,257.805	451,120.769	277.18420
42,482	2,417,259.805	451,196.769	278.000	2,417,259.805	451,196.769	279.44433
42,483	2,417,259.805	451,194.769	278.000	2,417,259.805	451,194.769	278.89585
42,484	2,417,259.805	451,192.769	278.000	2,417,259.805	451,192.769	278.28282

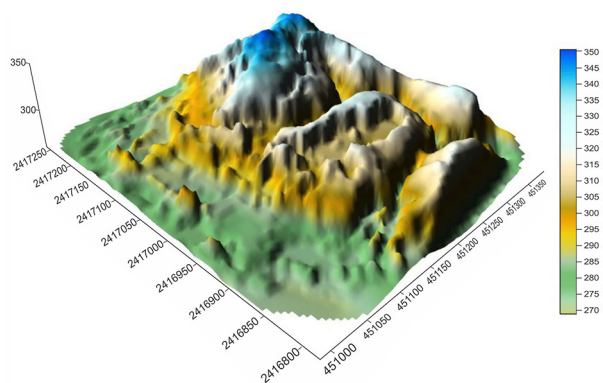


Fig. 9. Digital surface model of vegetation cover created by UAV technology

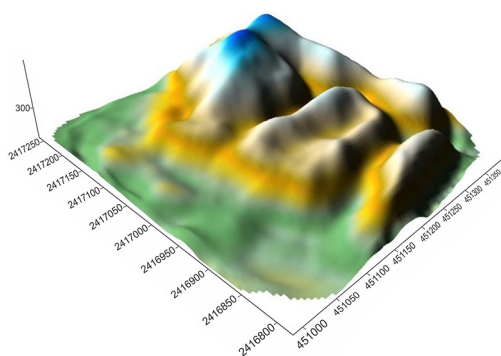


Fig. 10. The DSM model obtained after smoothing

sual and tabular evidence support an intermediate radius ( $\approx 50$  m) as a pragmatic balance for the present landscape.

**Polynomial fitting, canopy thickness estimation, and DEM derivation.** After DSM smoothing, the program computes local polynomial fits ( $2^{nd}$  or  $3^{rd}$  degree) using nearby checkpoints to model canopy thickness and predict bare-earth elevation per pixel. Table 3 reports the DEM points obtained after applying the correction procedure. The corrected elevations are generally lower than the smoothed DSM values, consistent with the removal of the canopy.

The magnitude of correction varies spatially and depends on canopy height and local slope (compare the smoothed DSM values in Table 2 and the corrected DEM values in Table 3). This two-stage approach (smoothing and local polynomial regression) thus separates the canopy signal from the terrain while leveraging the spatial constraints provided by GNSS checkpoints

The correction result to remove vegetation cover using the program module is the digital elevation model DEM, displayed in Fig. 11. The coordinates and elevations of the terrain points, after correcting for the thickness of the vegetation cover, are shown in Table 3.

**Quantitative accuracy assessment: effect of checkpoint number and smoothing radius.** Tables 4–6 quantify accuracy under combinations of smoothing radii ( $R = 0; 20; 50; 70; 100$  m) and checkpoint densities (150; 350; 1,000). Several clear patterns emerge.

The assessment of absolute accuracy and regulatory compliance (Table 4) confirms that the generated DEM meets recognized mapping standards. When using 1,000 checkpoints and a smoothing radius of 50 m, the DEM elevation errors relative to direct field measurements remain within the 1–2 m range reported in the

Coordinates and elevations of terrain points after removing vegetation cover

No.	Coordinates of the terrain point after removing vegetation cover		
	X, m	Y, m	H, m
1	2,416,951.805	451,202.769	303.94638
2	2,416,779.805	451,124.769	292.86742
3	2,416,779.805	451,122.769	292.37981
4	2,416,779.805	451,120.769	291.89517
5	2,416,779.805	451,118.769	290.42281
6	2,416,779.805	451,116.769	290.12016
7	2,416,779.805	451,114.769	289.87111
8	2,416,779.805	451,112.769	289.68769
9	2,416,779.805	451,110.769	289.5502
10	2,416,779.805	451,108.769	288.56795
...	...	...	...
42,470	2,417,257.805	451,142.769	269.70388
42,471	2,417,257.805	451,140.769	271.07127
42,472	2,417,257.805	451,138.769	272.27648
42,473	2,417,257.805	451,136.769	273.31903
42,474	2,417,257.805	451,134.769	274.22884
42,475	2,417,257.805	451,132.769	272.29549
42,476	2,417,257.805	451,130.769	294.43909
42,477	2,417,257.805	451,128.769	273.85668
42,478	2,417,257.805	451,126.769	259.93818
42,479	2,417,257.805	451,124.769	248.39593
42,480	2,417,257.805	451,122.769	243.00035
42,481	2,417,257.805	451,120.769	242.34133
42,482	2,417,259.805	451,196.769	251.8436
42,483	2,417,259.805	451,194.769	255.55988
42,484	2,417,259.805	451,192.769	259.38983

manuscript. This level of precision satisfies the typical accuracy requirements for large-scale topographic mapping at scales of 1:2,000 to 1:5,000, as defined by standard cartographic regulations. These results demonstrate that the integrated workflow, combining UAV-derived DSM acquisition, smoothing, and local polynomial correction anchored to CORS-based ground checkpoints, achieves operationally valid and regulatory-compliant accuracy, even in areas characterized by dense canopy cover and complex terrain.

The influence of checkpoint density shows a clear positive trend in improving DEM and DSM accuracy across all smoothing radii. As indicated in Table 5, the DSM root mean square error (RMSE) consistently decreases when the number of checkpoints increases from 150 to 1,000 for the same neighborhood radius. This improvement is intuitive and expected, as a higher checkpoint density offers a more detailed and representative ground reference for the local polynomial fitting process. Consequently, the model can better capture spatial variations in canopy thickness, thereby reducing interpolation and extrapolation errors and leading to more accurate estimates of ground elevation (DEM).

The analysis of the optimal smoothing radius (Table 6) demonstrates that a radius of approximately 50 meters provides the most balanced and accurate results. Specifically, the DEM–DSM differences after smoothing reach their minimum at this radius across all checkpoint densi-

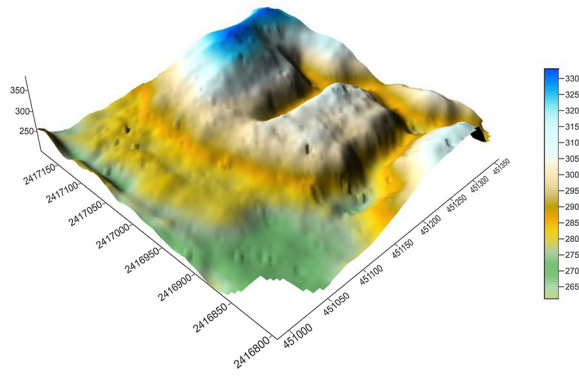


Fig. 11. Digital terrain model obtained after removing vegetation cover

ties. For example, when using 1,000 checkpoints, the difference between DEM and DSM at  $R = 50$  m is about 0.382 m, which is significantly smaller than at  $R = 0$  m ( $\approx 1.93$  m) or  $R = 100$  m ( $\approx 0.455$  m). This finding indicates that a 50 m smoothing radius effectively suppresses high-frequency canopy noise while still retaining essential terrain features. As a result, the subsequent polynomial fitting can estimate canopy thickness with high precision. Therefore,  $R = 50$  m represents the optimal compromise

between noise reduction and terrain preservation for this particular landscape and UAV sensor setup.

Sensitivity to radius extremes: at minimal radii ( $R = 0-20$  m), canopy noise remains significant and the DEM errors are higher; at enormous radii ( $R \geq 70-100$  m), micro relief is smoothed away, which can bias DEMs in areas with genuine rapid elevation change. Hence, the intermediate smoothing radius offers the best performance for landscapes with heterogeneous canopies and relief.

The empirical results demonstrate that the proposed method is robust and effective:

- an automated program module can ingest a UAV DSM, perform neighborhood smoothing, fit local polynomials against dense GNSS checkpoints and export corrected DEMs with diagnostic metrics (Figs. 6, 7);
- accuracy improves predictably with more checkpoints;
- the 50 m smoothing radius is empirically optimal for the Mai Pha site.

However, several limitations should be noted when interpreting these results.

First, sensor and image quality constraints arise from using the Phantom 3 Pro camera and JPEG-format imagery, which offer lower radiometric fidelity and

Table 4

Accuracy of elevation determination based on actual data

Smoothing radius, m	DEM model survey results, m					
	150 checkpoints		350 checkpoints		1,000 checkpoints	
	$m = \pm \sqrt{\frac{[\Delta\Delta]}{n}}$	$m = \pm \sqrt{\frac{[dd]}{2n}}$	$m = \pm \sqrt{\frac{[\Delta\Delta]}{n}}$	$m = \pm \sqrt{\frac{[dd]}{2n}}$	$m = \pm \sqrt{\frac{[\Delta\Delta]}{n}}$	$m = \pm \sqrt{\frac{[dd]}{2n}}$
$R = 0$	2.85777	2.02075	2.10068	1.48540	0.34218	0.24196
$R = 20$	2.61929	1.85212	1.82988	1.29392	0.27695	0.19583
$R = 50$	1.70805	1.20778	1.25556	0.88781	0.24959	0.17649
$R = 70$	1.84938	1.30771	1.29632	0.91663	0.25669	0.18151
$R = 100$	2.01114	1.42209	1.28005	0.90513	0.25543	0.18062

Table 5

Results of the accuracy assessment of the DSM surface digital model

Smoothing radius, m	DSM model survey results					
	150 checkpoints		350 checkpoints		1,000 checkpoints	
	$m = \pm \sqrt{\frac{[dd]}{n}}, m$	$m = \pm \sqrt{\frac{[dd]}{2n}}, m$	$m = \pm \sqrt{\frac{[dd]}{n}}, m$	$m = \pm \sqrt{\frac{[dd]}{2n}}, m$	$m = \pm \sqrt{\frac{[dd]}{n}}, m$	$m = \pm \sqrt{\frac{[dd]}{2n}}, m$
$R = 0$	4.13728	2.92550	3.26195	2.30655	0.66301	0.46882
$R = 20$	3.06931	2.17033	2.10725	1.49005	0.31197	0.22060
$R = 50$	1.74692	1.23526	1.24524	0.88052	0.25113	0.17758
$R = 70$	1.80750	1.27810	1.24958	0.88359	0.25331	0.17912
$R = 100$	1.91673	1.35533	1.24853	0.88284	0.24987	0.17668

Table 6

Accuracy assessment results between the DEM and DSM models after smoothing

Smoothing radius (m)	Smoothing radius of DEM and DSM models				
	$R = 0$ m	$R = 20$ m	$R = 50$ m	$R = 70$ m	$R = 100$ m
150 checkpoints	2.41986	1.38467	0.53938	0.48697	0.47078
250 checkpoints	2.36901	1.29053	0.47903	0.65780	0.43669
350 checkpoints	2.32869	1.15845	0.38612	0.34649	0.33662
1,000 checkpoints	1.93228	0.99312	0.38182	0.31917	0.45482

spatial resolution than dedicated metric cameras or LiDAR systems. Compression artifacts, rolling-shutter distortions, and motion blur may reduce tie-point density during structure-from-motion (SfM) processing, thereby affecting DSM precision.

Second, checkpoint logistics represent a practical challenge. While increasing checkpoint density improves accuracy, deploying and surveying as many as 1,000 reliable ground points can be costly and time-consuming, especially for larger or remote study areas. Therefore, the trade-off between field effort and desired accuracy must be carefully assessed for each mapping task.

Finally, heterogeneous vegetation structures and complex terrain, such as multi-layered forest canopies or steep, dissected slopes, may necessitate more adaptive approaches. In such cases, variable smoothing radii or more advanced canopy modeling techniques (structure-based height classification or LiDAR-assisted correction) could further enhance DEM reliability and terrain representation.

Based on the results of this study, several future directions can be proposed to enhance the performance, scalability, and applicability of the UAV-based DEM generation method. First, an adaptive smoothing and multi-scale fitting approach should be developed, allowing the smoothing radius to vary automatically according to local topographic complexity, slope, and canopy density. This would help retain important terrain details in steep or dissected areas while effectively reducing canopy-induced noise in flatter zones. Second, the integration of active sensors, such as UAV-mounted LiDAR or multispectral systems equipped with RTK/PPK positioning, would significantly improve ground-surface detection under dense vegetation and reduce the need for extensive ground control deployment. Third, incorporating machine learning algorithms, such as random forest, gradient boosting, or convolutional neural networks, could enable data-driven modeling of canopy thickness and enhance the precision of terrain correction, especially in areas where vegetation structure is complex or highly variable. Furthermore, it is essential to include uncertainty quantification in the DEM outputs by propagating the effects of checkpoint distribution, sensor geometry, and polynomial fitting errors, thereby increasing the reliability and interpretability of the resulting elevation products for engineering and environmental applications. Ultimately, future work should focus on optimizing operational workflows and cost-effectiveness by establishing guidelines that relate checkpoint density to expected accuracy, as well as automating ground control selection to reduce field workload. Collectively, these improvements would advance the current methodology toward a more adaptive, intelligent, and efficient framework for high-accuracy topographic mapping in complex terrain conditions.

**Conclusion.** The present study utilized UAV and GSNN technology to map dense vegetation areas in Lang Son Province, Vietnam. To achieve this, based on the theory of polynomial digital model problems, the study has developed a module to support the automatic correction of point heights determined by UAV digital image technology, combined with checkpoints established by CORS technology. Additionally, the research results have been compared with a digital elevation

model created from direct field measurement data using a total station to assess accuracy.

The study has smoothed the DSM model with different radius cases, such as 0; 20; 50; 70; and 100 m. At the same time, the results of the DEM model accuracy assessment are also determined for the cases of 150; 350; and 1,000 checkpoints, as well as the radius case. The findings indicate that the model's accuracy increases with the number of checkpoints. At the same time, depending on the type of vegetation cover surface, the elevation correction results from UAV image data will achieve the appropriate accuracy to create large-scale digital terrain maps.

The research results have been demonstrated experimentally, showing that the application of UAV digital imaging technology combined with dynamic GPS technology (RTK) in the survey work to establish large-scale digital topographic maps of 1,2000–1,5000, with a uniform height of 1 to 2 m in areas entirely covered by vegetation, ensures accuracy according to current regulations. The module of the program automatically corrects the elevation of points determined by UAV technology in areas covered by vegetation, which has both scientific and practical significance.

**Acknowledgments.** *We thank the anonymous reviewers and the editorial team for their valuable feedback on the earlier version, which helped us improve the manuscript's quality.*

#### References.

1. Ismael, R. Q., & Henari, Q. Z. (2019). Accuracy assessment of UAV photogrammetry for large scale topographic mapping. *2019 International Engineering Conference (IEC)*, 1-5. <https://doi.org/10.1109/IEC47844.2019.8950607>
2. Rovira-Más, F. (2011). Global 3D terrain maps for agricultural applications. *Advances in Theory and Applications of Stereo Vision*, 227-242. <https://doi.org/10.5772/13003>
3. Yu, M., Huang, Y., Xu, Q., Guo, P., & Dai, Z. (2016). Application of virtual earth in 3D terrain modeling to visual analysis of large-scale geological disasters in mountainous areas. *Environmental earth sciences*, 75, 1-7. <https://doi.org/10.1007/s12665-015-5161-5>
4. Ahmed, R., & Mahmud, K. H. (2022). Potentiality of high-resolution topographic survey using unmanned aerial vehicle in Bangladesh. *Remote Sensing Applications: Society and Environment*, 26, 100729. <https://doi.org/10.1016/j.rsase.2022.100729>
5. Latif, Z. A., Aman, S. N. A., & Pradhan, B. (2015). Landslide susceptibility assessment using high resolution Lidar-derived parameters and probabilistic frequency ratio model. *International Symposium on Multi-Hazard and Risk*, 72-84. Retrieved from [https://www.researchgate.net/publication/330439928\\_MJRSGIS\\_vol\\_4\\_num\\_2](https://www.researchgate.net/publication/330439928_MJRSGIS_vol_4_num_2)
6. Olsen, M. J., Johnstone, E., Driscoll, N., Ashford, S. A., & Kuester, F. (2009). Terrestrial laser scanning of extended cliff sections in dynamic environments: Parameter analysis. *Journal of Surveying Engineering*, 135(4), 161-169. [https://doi.org/10.1061/\(ASCE\)0733-9453\(2009\)135:4\(161\)](https://doi.org/10.1061/(ASCE)0733-9453(2009)135:4(161))
7. Darwin, N., Ahmad, A., & Akib, W. A. A. W. M. (2014). The potential of low altitude aerial data for large scale mapping. *Jurnal Teknologi (Sciences & Engineering)*, 70(5). <https://doi.org/10.1111/jt.v70.3523>
8. Colomina, I., & Molina, P. (2014). Unmanned aerial systems for photogrammetry and remote sensing: A review. *ISPRS Journal of photogrammetry and remote sensing*, 92, 79-97. <https://doi.org/10.1016/j.isprsjprs.2014.02.013>
9. Yazid, A., Wahid, R., Nazrin, K., Ahmad, A., Nasruddin, A., Rozilawati, D., & Razak, M. (2019). Terrain mapping from unmanned aerial vehicles. *Journal of Advanced Manufacturing Technology*, 13(1), 1-16. Retrieved from <https://jamt.utem.edu.my/jamt/article/view/5228>
10. Karantanellis, E., Marinos, V., Vassilakis, E., & Christaras, B. (2020). Object-based analysis using unmanned aerial vehicles (UAVs) for site-specific landslide assessment. *Remote Sensing*, 12(11), 1711. <https://doi.org/10.3390/rs12111711>
11. Aleshin, M., Gavrilova, L., & Melnikov, A. (2019). Use of unmanned aerial vehicles on example of Phantom 4 (standard) for creat-

- ing digital terrain models. *Engineering for Rural Development*, 22, 1686–1692. <https://doi.org/10.22616/ERDev2019.18.N488>
12. Taddia, Y., Stecchi, F., & Pellegrinelli, A. (2019). Using DJI Phantom 4 RTK drone for topographic mapping of coastal areas. *The International Archives of the Photogrammetry, Remote Sensing and Spatial Information Sciences*, 42, 625–630. <https://doi.org/10.5194/isprs-archives-XLII-2-W13-625-2019>
13. Ahmad, M., Ahmad, A., & Kanniah, K. (2018). Large scale topographic mapping based on unmanned aerial vehicle and aerial photogrammetric technique. *IOP Conference Series: Earth and Environmental Science*, 169(1), 012007. <https://doi.org/10.1088/1757-899X/305/1/012007>
14. Anguiano-Morales, M., Corral-Martínez, L., Trujillo-Schiaffino, G., Salas-Peimbert, D. P., & García-Guevara, A. E. (2018). Topographic investigation from a low altitude unmanned aerial vehicle. *Optics and Lasers in Engineering*, 110, 63–71. <https://doi.org/10.1016/j.optlaseng.2018.05.015>
15. Nwilag, B. D., Eyoh, A. E., & Ndehedehe, C. E. (2023). Digital topographic mapping and modelling using low altitude unmanned aerial vehicle. *Modeling Earth Systems and Environment*, 9(2), 1463–1476. <https://doi.org/10.1007/s40808-022-01677-z>
16. Lee, S., & Choi, Y. (2015). Topographic survey at small-scale open-pit mines using a popular rotary-wing unmanned aerial vehicle (drone). *Tunnel and underground space*, 25(5), 462–469. <https://doi.org/10.7474/TUS.2015.25.5.462>
17. Annis, A., Nardi, F., Petroselli, A., Apollonio, C., Arcangeletti, E., Tauro, F., & Grimaldi, S. (2020). UAV-DEMs for small-scale flood hazard mapping. *Water*, 12(6), 1717. <https://doi.org/10.3390/w12061717>
18. Watanabe, Y., & Kawahara, Y. (2016). UAV photogrammetry for monitoring changes in river topography and vegetation. *Procedia Engineering*, 154, 317–325. <https://doi.org/10.1016/j.proeng.2016.07.482>
19. Nazirova, A. B., Dubovenko, Y. I., Abdoldina, F. N., & Kuzminets, M. P. (2021). Optimization of GIS modules for processing data of gravity monitoring of subsoil. *Geoinformatics*, 1, 1–6. <https://doi.org/10.3997/2214-4609.20215521136>
20. Dubovenko, Y. I., Nazirova, A. B., & Abdoldina, F. N. (2022). Data-driven preprocessing of gravity data in oilfield GIS monitoring system. *International Conference Monitoring of Geological Processes and Ecological Condition of the Environment*, 1, 1–4. <https://doi.org/10.3997/2214-4609.2022580267>
21. Meng, X., Shang, N., Zhang, X., Li, C., Zhao, K., Qiu, X., & Weeks, E. (2017). Photogrammetric UAV mapping of terrain under dense coastal vegetation: An object-oriented classification ensemble algorithm for classification and terrain correction. *Remote Sensing*, 9(11), 1187. <https://doi.org/10.3390/rs9111187>
22. Choi, S. K., Ramirez, R. A., & Kwon, T. H. (2023). Acquisition of high-resolution topographic information in forest environments using integrated UAV-LiDAR system: System development and field demonstration. *Heliyon*, 9(9), e20225. <https://doi.org/10.1016/j.heliyon.2023.e20225>

## Великомасштабне топографічне картографування районів із рослинністю на основі технологій БПЛА та GNSS

Тхуї Тхі Хоанг, Ань Туан Луу\*

Ханойський університет гірничої справи та геології, факультет геоматики та землеустрою, м. Ханой, Соціалістична Республіка В'єтнам

\* Автор-кореспондент e-mail: [luuanhtuan@hmg.edu.vn](mailto:luuanhtuan@hmg.edu.vn)

**Мета.** Розроблення методу побудови високоточної великомасштабної топографічної карти в ра-

йонах із густою рослинністю із використанням технологій БПЛА (безпілотних літальних апаратів) і GNSS (глобальних навігаційних супутникових систем). Основна увага приділена корекції висотних даних, отриманих із зображень БПЛА, за допомогою поліноміальної моделі на основі контрольних пунктів мережі CORS.

**Методика.** Дослідження виконано в комуні Май Фа, провінція Лангшон, В'єтнам. Для зйомки аерофото зображень використовувався БПЛА DJI Phantom 3 Pro, а для збирання наземних опорних точок застосовували технологію GNSS-RTK (CORS). Для моделювання товщини рослинного покриву й корекції цифрової моделі поверхні (DSM) з метою отримання цифрової моделі рельєфу (DEM) застосовано метод апроксимації поліноміальною поверхнею (1–3-го ступеня). DSM згладжувалася із використанням різних радіусів фільтрації (0; 20; 50; 70; 100 м), а точність оцінювалася при різній кількості контрольних пунктів (150; 350; 1 000). Розроблено програмний модуль для автоматизації процесу корекції.

**Результати.** Точність DEM зростала зі збільшенням кількості контрольних пунктів і правильно підібраним радіусом згладжування. Найкращих результатів досягнуто при використанні 1 000 контрольних пунктів і радіусу згладжування 50 м. Скоригована DEM забезпечила точність за висотою на рівні 1–2 метрів, що відповідає нормативним вимогам до великомасштабних топографічних карт (1:2 000–1:5 000). Запропонований метод продемонстрував ефективність навіть у районах із густою рослинністю, де традиційні методи зйомки мають обмеження.

**Наукова новизна.** У роботі запропоновано новий підхід, що інтегрує фотограмметрію БПЛА із даними GNSS-RTK і поліноміальним моделюванням поверхні для корекції висотної інформації в районах із рослинним покривом. Створений програмний модуль автоматизує процес корекції, підвищуючи його ефективність та однорідність.

**Практична значимість.** Запропонований метод забезпечує можливість створення точних великомасштабних цифрових топографічних карт у складних умовах густої рослинності. Він є економічно ефективною й продуктивною альтернативою традиційним методам зйомок і має потенційне застосування в лісовому господарстві, землекористуванні та плануванні інфраструктури.

**Ключові слова:** БПЛА, технологія GNSS, райони з рослинністю, великомасштабна топографічна карта

*The manuscript was submitted 24.10.25.*